The Canadian Mineralogist
Vol. 50, pp. 1265-1280 (2012)
DOI: 10.3749/canmin.50.5.1265

LAURENTIANITE, $[NbO(H_2O)]_3(Si_2O_7)_2[Na(H_2O)_2]_3$, A NEW MINERAL FROM MONT SAINT-HILAIRE, QUEBEC: DESCRIPTION, CRYSTAL-STRUCTURE DETERMINATION AND PARAGENESIS

MONIKA M.M. HARING AND ANDREW M. MCDONALD§

Department of Earth Sciences, Laurentian University, Sudbury, Ontario P3E 2C6, Canada

MARK A. COOPER

Department of Geological Sciences, University of Manitoba, Winnipeg, Manitoba R3T 2N2, Canada

GLENN A. POIRIER

Research Division, Canadian Museum of Nature, P.O. Box 3443, Station D, Ottawa, Ontario K1P 6P4, Canada

ABSTRACT

Laurentianite, $[NbO(H_2O)]_3(Si_2O_7)_2[Na(H_2O)_2]_3$, is a new mineral discovered in siderite-dominant pods in an altered syenite at the Poudrette quarry, Mont Saint-Hilaire, Quebec. Crystals are colorless, acicular, euhedral, and elongate along [001] with average dimensions of 0.012 × 0.012 × 0.25 mm. The mineral generally occurs in loose, randomly oriented groupings ('nests') of crystals. Associated minerals include quartz, pyrite, franconite, rutile, lepidochrocite, and an unidentified Fe-bearing mineral. Laurentianite is transparent to translucent with a vitreous luster and is non-fluorescent under long-, medium-, and short-wave radiation. The Mohs hardness could not be measured owing to the small size of the crystals. No partings or cleavages were observed, although crystals do exhibit a splintery fracture. The calculated density is 2.464 g/cm^3. Laurentianite is nonpleochroic and uniaxial negative, with ω 1.612(2) and ε 1.604(2). The average of 12 analyses from several crystals is: Na_2O 8.88 (4.54–12.80), K_2O 0.26 (0.14–0.44), CaO 0.22 (0.10–0.43), TiO_2 0.58 (0.31–0.83), Nb_2O_5 43.64 (36.43–49.90), SiO_2 26.87 (22.81–29.07), and H_2O (calc.) 17.93, total 98.38 wt.% on the basis of 26 anions, corresponding to $[(Nb_{0.99}Ti_{0.01})_{\Sigma 1.00}O(H_2O)]_3(Si_{2.00}O_7)_2[(Na_{0.86}\square_{0.10}K_{0.02}Ca_{0.01})_{\Sigma 0.99}(H_2O)_2]_3$ or, ideally, $[NbO(H_2O)]_3(Si_2O_7)_2[Na(H_2O)_2]_3$. The presence of H_2O in laurentianite is inferred from Raman spectroscopy and results from refinement of the crystal structure. The mineral crystallizes in space group *P*3 (#143) with *a* 9.937(1), *c* 7.004(1) Å, *V* 599.0(1) Å^3, and *Z* = 1. The strongest six lines on the X-ray powder-diffraction pattern [*d* in Å (I) (*hkl*)] are: 8.608 (100) (010), 7.005 (19) (001), 4.312 (25) (020), 3.675 (25) (201, 021), 3.260 (31) (120, 210), and 2.870 (20) (030). The crystal structure of laurentianite, refined to $R = 2.78\%$ for 2347 reflections ($F_o > 4\sigma F_o$) contains one *Na*, two *Nb*, and four *Si* sites. The two *Nb* sites are coordinated in distorted $NbO_5(H_2O)$ octahedra, with four equatorial bonds of typical Nb–O bond distances (~2 Å) and two highly asymmetric ones (one long, ~2.5 Å and one short, ~1.8 Å). Each site is each only partially occupied (~50%) and because of the short distance between them (~0.7 Å), they are not simultaneously occupied. A novel cation-anion coordination scheme involving the apical oxygens, Nb, and disordered H_2O groups is developed: when one of the *Nb* sites is occupied, the other is vacant, resulting in one of the apical O sites being occupied by O^{2-} and the other by H_2O. The opposite situation occurs when the occupancy and vacancy of the *Nb* sites are reversed, leading to both apical O sites having an equal, mixed (O^{2-}/H_2O) composition. A minor charge understaturation at both apical O sites is remedied by each of these O sites receiving a single H-bond from one of the H_2O groups associated with the Na cation.

The crystal structure of laurentianite is based on five-membered pinwheels of composition $[Nb_3Si_2O_{17}(H_2O)_3]^{-11}$, consisting of three $NbO_5(H_2O)$ octahedra linked to two SiO_4 tetrahedra. Individual Nb–Si pinwheels are attached to form a layer composed of 18-membered rings of composition $[Nb_6Si_{12}O_{54}(H_2O)_6]^{30-}$ perpendicular to [001]. The crystal structure is also layered along [001], with a silicate layer composed of (Si_2O_7) dimers and a layer of isolated $NbO_5(H_2O)$ octahedra. Sodium atoms are positioned within the silicate layer, occupying sites that almost directly overly the *Nb* sites but are displaced ~*z* + ½. Laurentianite is a late-stage mineral intergrown with lepidocrocite, both of which overgrow franconite and quartz. The mineral is believed to have precipitated from a late-stage aqueous fluid enriched in Na, Si, and Nb, possibly arising through the breakdown of franconite, sodalite, and quartz.

Keywords: laurentianite, Mont Saint-Hilaire, crystal structure, altered syenite, niobium silicate, Raman spectroscopy, silicate layers, distorted octahedra, paragenesis

§ *E-mail address*: amcdonald@laurentian.ca

Introduction

A key feature of agpaitic geological environments like those found in Langesundsfjorden (Norway), the Kola Peninsula (CIS), and Mont Saint-Hilaire (Canada) is the occurrence of silicate minerals containing essential quantities of high-field strength elements (HFSE). Most frequently, these minerals are dominated by Zr (*e.g.*, eudialyte-group minerals) and Ti (*e.g.*, labuntsovite-group minerals) and only rarely by Nb (*e.g.*, vuonnemite). Given the relative abundances of both Zr and Ti, the majority of HFSE-bearing minerals found in agpaitic environments are dominated by these, with those containing essential Nb being rarer. Therefore, while discoveries of new species containing essential Zr or Ti are not typically uncommon, those involving minerals that contain essential Nb are much less so, and are thus deserving of greater attention.

As part of an ongoing study of the mineralogy of the agpaitic rocks at Mont Saint-Hilaire, a new Nb-dominant mineral, laurentianite, $[NbO(H_2O)]_3(Si_2O_7)_2[Na(H_2O)_2]_3$, has been discovered and is characterized in this present contribution, along with data pertaining to its paragenesis. Samples containing laurentianite were originally recovered by Mrs. Hanna Vestergaard of Brampton, Ontario, Canada, who collected them from a waste pile in the southeast corner of the Poudrette quarry at Mont Saint-Hilaire, Quebec. The mineral was submitted to one of us (AMM) for identification, but as its chemical composition and X-ray powder diffraction pattern did not match those of any known mineral, it was temporarily designated UK 117. Subsequent analyses confirmed it to be new to science. It has been named after Laurentian University, Sudbury, Ontario, Canada (established 1963), where the research characterizing this mineral as a new species was conducted. Both the mineral and its name have been approved by the Commission of New Minerals and Mineral Names (CNMMN), IMA (2010-018). The holotype material is a matrix sample (3.5 × 2.5 × 1.0 cm) and is housed in the collection of the Royal Ontario Museum, Toronto, under catalogue number M55369.

Occurrence

Samples containing laurentianite were collected from the Poudrette quarry, Rouville RMC, Montérégie (formerly Rouville County), Quebec, Canada. They were not found *in situ*, but rather, in a highly oxidized waste-rock pile located in the southeast corner of the quarry, on 6 September, 2003. The samples consist predominantly of siderite (>90 modal %) which develops as aggregates of euhedral crystals. Individual siderite crystals average 3 mm in size (maximum 6 mm) and are strongly color zoned (typically with dark brown cores and lighter brown to tan rims). They are euhedral, strongly flattened on [0001], exhibit the form pinacoid {0001} (dominant) and two minor, unidentified rhombohedra. Quartz is the second most abundant mineral present (8 modal %). It develops as grey (common) to light-brown (rare), euhedral crystals averaging 2 mm in length (maximum 5 mm). Individual crystals are dominated by equally developed rhombohedra $\{10\bar{1}1\}$ and $\{01\bar{1}1\}$ (major) and the prism $\{10\bar{1}0\}$ (minor) being present. Crystals have a noticeably greasy to dull luster, possibly owing to a partial dissolution of crystal faces. The remainder of the sample is predominantly made up of franconite ($Na_2Nb_4O_{11}\cdot 9H_2O$; 2 modal %). It occurs in aggregates of ellipsoidal spherules (up to 1.5 mm) composed of acicular, bladed, radiating crystals. Additional trace phases include rutile (aggregates up to 1 mm composed of black, lustrous, bladed crystals that average 0.1 mm in length), pyrite (developing either as isolated or aggregates of brassy yellow, euhedral crystals with the form cube {100}, commonly in the interstices between siderite crystals), albite (clear, colorless, tabular, bladed crystals up to 0.2 mm in length), and reddish-brown lepidochrocite (identified by a combination of energy-dispersive spectrometry and Raman spectroscopy), the latter coating much of the specimens recovered. In addition, an unidentified, bright yellow, Fe-bearing mineral (possibly a Fe-oxy-hydroxide) has been observed, generally occurring as fine-grained coatings on and in siderite, and only rarely as equant, euhedral crystals averaging 0.1 mm across. Many of the siderite crystals have developed a cavernous appearance due to partial dissolution and it is in such cavities that euhedral crystals of the unidentified yellow Fe-bearing mineral occur, along with rare pyrite. Powder X-ray diffraction patterns from the unidentified mineral contain numerous lines, but a combination of sharp and diffuse diffraction lines are noted, suggesting it may not be completely crystalline. Studies are ongoing to verify the nature of this material.

Physical and Optical Properties

Crystals of laurentianite are euhedral to subhedral, acicular, and elongate along [001], occurring in randomly oriented, loosely packed groupings or 'nests' (Fig. 1). They exhibit the prominent forms trigonal prism $\{10\bar{1}0\}$ (dominant) and pedion {0001} (very minor). Crystals have average dimensions of 0.012 × 0.012 × 0.15 mm and average length-to-width ratios of 12.5. The mineral is transparent to translucent, and colorless (crystals may exhibit a reddish hue owing to overgrowths of lepidochrocite) with a white streak. It has a vitreous to satiny luster and shows no fluorescence under short-, medium-, or long-wavelength radiation. Due to the small size of the crystals, the Mohs hardness could not be measured. A density of 2.464 g/cm^3 was calculated using the empirical chemical formula and unit-cell parameters derived from the crystal-structure analysis.

Laurentianite is non-pleochroic, uniaxial negative with ω 1.612(2) and ε 1.604(2), as measured with a

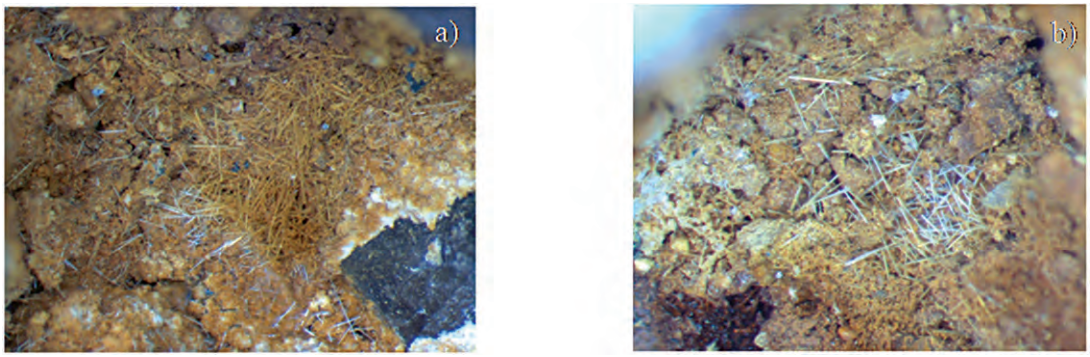

FIG. 1. Loose aggregates of laurentianite (a) intergrown with lepidochrocite (FOV: 2.0 mm) and (b) without lepidochrocite (FOV: 1.5 mm).

Na-vapor lamp (λ = 589 nm). The Gladstone-Dale calculation, using the empirical formula as well as unit-cell parameters derived from the crystal structure analysis, gives a compatibility index of 0.042, considered good (Mandarino 1981).

CHEMICAL COMPOSITION

Laurentianite was analyzed with a JEOL 733 Superprobe using an operating voltage of 15 kV, a beam current of 5 nA, and a beam width of 10 μm. A relatively narrow beam width was employed because of the extremely small size of the crystals. Wavelength-dispersive data were collected using the following standards: albite (Na*K*α), diopside (Ca*K*α, Si*K*α), sanidine (K*K*α), hematite (Fe*K*α), rutile (Ti*K*α), and Mn-columbite (Nb*L*α). Also sought, but not detected, were Sr, Ba, Mg, Mn, Al, Zr, Ta, and F. Twelve analyses were obtained from several crystals, giving an average of: Na_2O 8.88(4.54–12.80), K_2O 0.26 (0.14–0.44), CaO 0.22 (0.10–0.43), TiO_2 0.58 (0.31–0.83), Nb_2O_5 43.64 (36.43–49.90), SiO_2 26.87 (22.81–29.07), and H_2O (calc.) 17.93, total 98.38 wt.%. Iron was found in highly variable concentrations (from below detection up to 1.04 wt.% FeO_{total}). Given the intimate intergrowth of laurentianite with lepidocrocite, the presence of Fe is considered attributable to the latter and was thus excluded from the empirical formula for laurentianite. The presence of H_2O was established *via* the results of crystal-structure and Raman analyses (see below). The mineral is unstable under the electron beam, a likely explanation for the variations observed in the major element oxide totals. The empirical formula, based on 26 anions, is $[(Nb_{0.99}Ti_{0.01})_{\Sigma 1.00}O(H_2O)]_3(Si_{2.00}O_7)_2[(Na_{0.86}\square_{0.10}K_{0.02}Ca_{0.01})_{\Sigma 0.99}(H_2O)_2]_3$ or, ideally, $[NbO(H_2O)]_3(Si_2O_7)_2[Na(H_2O)_2]_3$. We have chosen to present the formula in this relatively unconventional manner as it (1) reflects the essential chemical components of the mineral and (2) provides a succinct view of the crystal structure of the mineral. The ideal formula requires: Na_2O 10.40, Nb_2O_5 44.59, SiO_2 26.88, H_2O 18.13 wt.%, total 100.00 wt.%. Laurentianite does not effervesce in 10% HCl at room temperature. It is particularly noteworthy that laurentianite is effectively devoid of Ta, at least at the level of EMPA-type analyses (estimated minimum detection limits of 800–1700 ppm under typical conditions, *i.e.*, 25 s at 20 nA) given: (1) the crystal-chemical similarity of Nb and Ta [owing to their identical charges (5+) and similar radii (0.64 Å) for [6]; Shannon, 1976]; (2) that the two do not appear to undergo significant fractionation during most magmatic and metamorphic processes (Babechuk & Kamber 2011); and (3) that average Nb/Ta ratios are typically on the order of 10–20 [*e.g.*, bulk silicate Earth: ~18, corresponding to a C1 chondrite (Jochum *et al.* 2000); continental crustal ~12–13 (Barth *et al.* 2000); and depleted mantle, ~16 (Jochum *et al.* 2000)]. Thus, the fluids from which laurentianite crystallized must have undergone extreme Nb/Ta fractionation at some stage. While this decoupling of Nb from Ta is intriguing from a crystal-chemical perspective, it does appear to be a key feature of agpaitic environments (*e.g.*, Kola Peninsula, CIS; Larvik Plutonic Complex, Norway, *etc.*), unlike the situation in silica-saturated systems, where oxides containing both Nb and Ta may be found (*e.g.*, columbite-group minerals). This, therefore, suggests the existence of a hereto-unrecognized type of geochemical process(es) related to the formation of agpaitic rocks.

RAMAN ANALYSIS

The Raman spectrum (average of three 30 s spectra) of a single crystal of laurentianite was obtained over the range of 50 to 4000 cm^{-1} (Fig. 2). Data were collected in backscattered mode with a HORIBA Jobin Yvon XploRA spectrometer interfaced with an Olympus BX 41 microscope, 100× magnification (estimated spot size of 2 μm), a 1200 grating, and an excitation radiation of

532 nm. Calibration was made using the 521 cm^{-1} line of Si in a silicon wafer. The spectrum is dominated by two sharp absorption peaks at 920 and 841 cm^{-1}, corresponding to the internal stretching modes (symmetrical) of $Si–O_{nbr}$. As there are four unique Si atoms with two pairs having very similar fractional coordinates, it is likely that each of these two peaks is a doublet. There are also three broad peaks at 3024, 3327, and 3421 cm^{-1}, corresponding to the O–H stretching of H_2O groups. The H–O–H absorption band (H_2O bend), which would be expected to occur at ~1600 cm^{-1}, was not observed. Its absence can be ascribed to a combination of the inherent weakness of this band by Raman spectroscopy in general and possibly grain orientation (the intensity of a Raman-active band can be strongly dependent on the orientation of the species being activated). Outside of these, the spectrum contains numerous weak absorption bands, particularly in the region below 800 cm^{-1} (Fig. 2, inset). Those observed at 700 and 771 cm^{-1}, along with 244 and 302 cm^{-1}, are ascribed to Nb–O vibrations, based on data from Rocha *et al*. (1996) for synthetic Ti-Nb-silicates related to nenadkevichite. As considerable overlap exists between lower frequency Na–O and Nb–O absorption bands, no attempt was made to assign those present in the region between ~310 and 100 cm^{-1}. Table 1 lists the suggested assignments for all the observed absorption bands present in the Raman spectrum for laurentianite.

TABLE 1. OBSERVED ABSORPTION BANDS AND BAND ASSIGNMENTS FOR THE RAMAN SPECTRUM OF LAURENTIANITE

Raman Absorption Band (cm^{-1})	Suggested Assignment
3421 m	Stretching mode of H_2O
3327 m	"
3024 m	"
1103 vw	Asymmetric stretching mode of $Si–O_{nbr}$
1054 vw	"
929 vs	Symmetric stretching mode of $Si–O_{br}$
841 vvs	"
771 w	Nb–O vibrations
700 w	"
628 vvw	Symmetric bending mode of $Si–O_{br}$
597 w	"
560 vvw	"
486 w	Asymmetric bending mode of $Si–O_{br}$
467 w	"
405 m	"
344 vw	Unassigned
309 m	Nb–O and Na–O vibrations
292 m	"
241 m	"
218 m	"
193 m	"
176 m	"
138 w	"
122 m	"
90 m	Na–O

Note: vvs = very very strong, vs = very strong, m = medium, w = weak,vw = very weak, vvw = very very weak.

X-Ray Crystallography and Crystal-Structure Determination

X-ray powder diffraction data was collected using a 114.6 mm diameter Gandolfi camera, 0.3 mm colli-

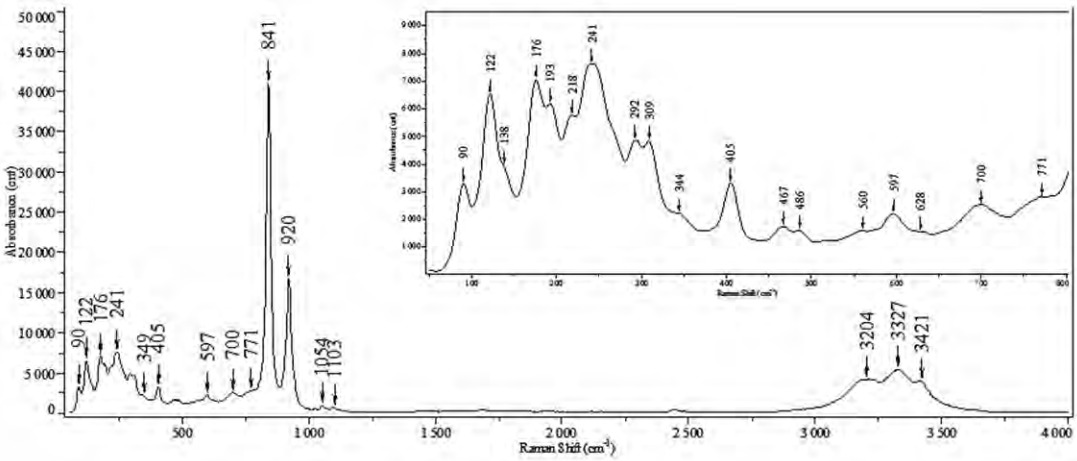

FIG. 2. Raman spectrum for laurentianite with absorption peaks indicated. An expanded view of the region from 50 to 800 cm^{-1} is provided in the inset.

mator, and Fe-filtered Co$K\alpha$ radiation (λ = 1.7902 Å). Intensities were determined using a scanned image of the powder pattern and normalization to the measured intensity of d = 8.608 Å (I = 100). To determine how much an *hkl* plane contributed to a reflection, the measured intensities were compared to a pattern calculated using results from the crystal-structure analysis and the program CRYSCON (Dowty 2002). Overall, there is a good agreement between the measured and calculated powder patterns (Table 2).

X-ray intensity data were collected with a Bruker D8 three-circle diffractometer equipped with a rotating-anode generator, multi-layer optics incident beam path and an APEX-II CCD detector. In excess of a sphere of X-ray diffraction data (20894 reflections) was collected to 60° 2θ using 30 s per 0.2° frame with a crystal-to-detector distance of 5 cm. The unit-cell parameters were obtained by least-squares refinement of 9903 reflections ($I > 10\sigma I$), and are given in Table 3. Empirical absorption corrections (SADABS; Sheldrick 1997) were applied and identical data merged to give 6993 reflections covering the entire Ewald sphere. Information pertaining to the data collection is given in Table 3.

Solution and refinement of the crystal structure of laurentianite were done using the SHELX-97 package of programs (Sheldrick 1997), neither of which were straightforward. First, although a cell of dimensions ~ 10 × 10 × 7 Å has been adopted, there are addi-

TABLE 2. LAURENTIANITE X-RAY POWDER DIFFRACTION DATA

I_{meas}	I_{calc}	d_{meas}(Å)	d_{calc}(Å)	h	k	l	I_{meas}	I_{calc}	d_{meas}(Å)	d_{calc}(Å)	h	k	l
100	**100**	**8.608**	**8.6057**	**0**	**1**	**0**	3	2	1.4769	1.4750	2	4	2
19	**22**	**7.005**	**7.004**	**0**	**0**	**1**	1	<1	1.4652	1.4633	1	4	3
5	4	5.445	5.4322	0	1	1	2	1	1.4340	1.4343	0	6	0
5	<1	4.976	4.9685	1	1	0		2		1.4312	2	2	4
25	**22**	**4.312**	**4.3028**	**0**	**2**	**0**	3	<1	1.4153	1.4148	3	4	0
13	8	4.062	4.0524	1	1	1	1	<1	1.3793	1.3780	2	5	0
25	**29**	**3.675**	**3.6663**	**0**	**2**	**1**	1	<1	1.3533	1.3521	2	5	1
31	**23**	**3.260**	**3.2526**	**1**	**2**	**0**	1	<1	1.3347	1.3345	2	4	3
6	2	2.957	2.9501	1	2	1		2		1.3320	2	0	5
20	**2**	**2.870**	**2.8686**	**0**	**3**	**0**	2	<1	1.3132	1.3124	1	6	0
	11		**2.8624**	**1**	**1**	**2**	2	<1	1.2907	1.2899	1	6	1
12	18	2.723	2.7161	0	2	2	1	<1	1.2841	1.2823	2	5	2
1	8	2.490	2.4842	2	2	0	1	1	1.2438	1.2421	4	4	0
6	<1	2.390	2.3868	1	3	0	2	<1	1.2310	1.2294	0	7	0
1	1	2.346	2.3413	2	2	1		2		1.2294	3	5	0
5	<1	2.264	2.2592	1	3	1	2	<1	1.2121	1.2109	0	7	1
4	3	2.156	2.1514	0	4	0		<1		1.2109	3	5	1
1	3	2.117	2.113	1	1	3	1	<1	1.2051	1.2032	3	3	4
2	2	2.058	2.0566	0	4	1	1	<1	1.1926	1.1934	2	6	0
	2		2.0521	2	0	3	4	<1	1.1605	1.1600	0	7	2
4	2	2.030	2.0262	2	2	2		<1		1.1600	3	5	2
11	4	1.976	1.9743	2	3	0	1	<1	1.1443	1.144	1	6	3
	2		1.9723	3	1	2	2	2	1.1262	1.1266	0	2	6
1	<1	1.900	1.9002	2	3	1		2		1.1096	6	0	4
1	<1	1.881	1.8779	1	4	0	2	<1	1.0857	1.0864	0	5	5
14	14	1.836	1.8331	0	4	2	1	<1	1.0710	1.0715	3	6	1
3	<1	1.816	1.8139	1	4	1	1	<1	1.0510	1.051	4	5	2
1	<1	1.722	1.7211	0	5	0	1	<1	1.0388	1.0379	1	5	5
	2		1.7158	1	0	4	1	2	1.0253	1.026	0	4	6
1	1	1.704	1.7013	2	2	3	1	1	1.0138	1.0131	4	4	4
3	<1	1.671	1.6714	0	5	1	4	<1	1.0069	1.0072	1	8	0
4	<1	1.657	1.6562	3	3	0		<1		1.007	2	7	2
1	<1	1.625	1.6263	2	4	0	1	<1	0.9844	0.9838	5	5	1
	2		1.6219	2	0	4	2	<1	0.9687	0.9682	3	7	0
1	<1	1.614	1.6117	3	3	1	3	<1	0.9569	0.9563	1	2	7
2	<1	1.5851	1.5842	2	4	1	2	2	0.9487	0.9483	2	4	6
	2		1.5821	4	0	3	1	<1	0.9324	0.9326	4	5	4
3	2	1.5471	1.5456	1	5	0	5	2	0.9243	0.924	0	7	5
3	<1	1.5111	1.5093	1	5	1		<1		0.924	3	5	5
3	1	1.4989	1.4972	3	3	2	1	<1	0.9166	0.9166	0	8	4

Table 3. Miscellaneous data for laurentianite

a (Å)	9.937(1)	Criterion for observed	
c	7.004(1)	reflections	$F_o > 4\sigma(F_o)$
V (Å^3)	599.0(1)	GoOF	1.099
Space group	*P*3 (#143)	Total No. of reflections	20894
Z	1	No. Unique reflections	2347
D_{calc} (g/cm^{-3})	2.464	*R*(merge %)	2.52
Radiation	Mo*K*α	*R* (%)	2.78
	(50 kV, 24 mA)	wR^2 (%)	7.94

tional observed (commensurate) data that suggest the existence of a larger cell of dimensions 10 × 10 × 42 Å (*i.e.*, one with a cell edge of 6*c*). While models assuming both unit cells were considered, a successful interpretation of the crystal structure of laurentianite could only be obtained with the smaller cell. However, that the mineral actually possesses a larger unit cell must still be considered a possibility. The crystal structure of laurentianite was solved by direct methods, using the scattering curves of Cromer & Mann (1968) and the scattering factors of Cromer & Liberman (1970). Phasing of a set of normalized structure-factors gave a mean $|E^2 - 1|$ value of 0.804, inconclusive as to whether the mineral is centrosymmetric or non-centrosymmetric. From a listing of potential space-groups consistent with the observed diffraction character of the mineral, and in light of preliminary data that suggested the mineral was likely non-centrosymmetric, space-group *P*3 (#143) was chosen. Phase-normalized structure factors were used to give an *E*-map from which two *Nb*, four *Si*, and several *O* sites were located. The site assigned to *Na* was located from subsequent *E*-maps. Determination of which sites were occupied by O or H_2O was based on bond-valence calculations as well as electroneutrality considerations. This model resulted in two *Nb* sites, *Nb*1 and *Nb*1, separated by 0.725(1) Å along *y*. The short distance between the two *Nb* sites precludes both being occupied simultaneously. Refinement of the site-occupancy factors (*SOF*) converged to 0.55(1) for *Nb*1, to 0.45(1) for *Nb*2, and to 0.92(1) for the *Na* site, the latter being consistent with results from the EMP analyses. Refinement of this model converged to R = 6.10% and wR^2 = 20.37% with a Flack *x* parameter of 0.5(1). Considering these less-than-ideal results, the fact that the mineral crystallizes in a trigonal space group (notorious for frequently being twinned), and examination of the derived crystal structure (which suggests two-fold axes along [100]), it was deduced that the crystal analyzed might be a merohedral twin. Inclusion of the twin matrix [0$\bar{1}$0/$\bar{1}$00/001] to compensate for the apparent introduction of a two-fold rotation axis along [100] was made and refinement of the crystal structure significantly improved, producing final residuals of R = 2.78% and wR^2 = 7.94% and the highest value on difference map calculated at this stage being 0.49 e$^-$/Å. Models of higher symmetry (notably those in the hexagonal system) were also considered but none proved to be consistent with the observed atomic arrangement, in particular, with the highly distorted *Nb*$O_5(H_2O)$ octahedra (~1.8 Å and ~2.5 Å apical ligands, and four equatorial ligands at ~2 Å, as is discussed below). Given the high degree of disorder and partial occupancies associated with H_2O groups present in the mineral, identification of potential H positions from difference-Fourier maps were not considered as being reliable and were thus not included in the refinement. Information pertaining to data collection and crystal-structure refinement is given in Table 3, positional and displacement parameters in Table 4, selected interatomic distances in Table 5 and a bond-valence analysis in Table 6. Observed and calculated structure factors are available from The Depository of Unpublished Data, CISTI, National Research Council, Ottawa, Ontario, K1A 0S2, Canada, and also from the Depository of Unpublished Data on the Mineralogical Association of Canada website (Laurentianite CM50_1265).

Crystal Structure

Coordination of the cations

There are four unique SiO_4 tetrahedra, each bonded to three equivalent and one non-equivalent O. The former serve as bonds with Nb and the latter as linkages between Si_2O_7 groups that develop along [001] (*Si*1 and *Si*2 are linked through *O*1, *Si*3 and *Si*4 are linked through *O*4, with the remaining bonds for both *O*1 and *O*4 being made solely with Na). The SiO_4 tetrahedra all have normal <Si–O> bond distances ranging from 1.601 to 1.613 Å (Table 5).

There are two *Nb* sites, *Nb*1 and *Nb*2, each ~50% occupied, and both cannot be occupied simultaneously. The two sites are each coordinated in a very interesting distorted *Nb*$O_5(H_2O)$ octahedron with four equatorial *Nb*–O bonds of typical length (1.95–2.00 Å), and two highly asymmetric apical bonds: one very short, ~1.78 Å, and the other quite long, ~2.50 Å, the latter being possibly the longest Nb–O bond observed in a mineral (Fig. 3). The only other mineral with a similar $O_5(H_2O)$ octahedral coordination of Nb^{5+} is epistolite, with four

TABLE 4. POSITIONAL AND DISPLACEMENT PARAMETERS FOR LAURENTIANITE

atom	*x*	*y*	*z*	SOF	U_{11}	U_{22}	U_{33}	U_{23}	U_{13}	U_{12}	U_{eq}
*Na*1	0.3304	0.1644	1.2429	0.92	0.0262	0.0311	0.0122	–0.0055	–0.0002	0.0133	0.0236
	0.0006	0.0004	0.0009	0.01	0.0007	0.0011	0.0007	0.0009	0.0004	0.0010	0.0005
*Nb*1	0.3326	0.1293	0.7482	0.55	0.0108	0.0156	0.0011	0.0019	–0.0001	0.0055	0.0097
	0.0001	0.0001	0.0002	0.01	0.0003	0.0004	0.0003	0.0003	0.0002	0.0004	0.0002
*Nb*2	0.3322	0.2015	0.7389	0.45	0.0116	0.0162	0.0120	–0.0001	–0.0002	0.0060	0.0137
	0.0002	0.0002	0.0003	0.01	0.0005	0.0006	0.0006	0.0004	0.0003	0.0005	0.0003
*Si*1	2/3	1/3	1.0157	1	0.0114	0.0114	0.0029	0	0	0.0057	0.0086
			0.0004		0.0009	0.0009	0.0011			0.0004	0.0005
*Si*2	2/3	1/3	1.4783	1	0.0123	0.0123	0.0021	0	0	0.0062	0.0089
			0.0003		0.0009	0.0009	0.0013			0.0004	0.0006
*Si*3	0	0	1.0161	1	0.0126	0.0126	0.0048	0	0	0.0063	0.0100
			0.0003		0.0009	0.0009	0.0013			0.0004	0.0006
*Si*4	0	0	1.4780	1	0.0136	0.0136	0.0039	0	0	0.0068	0.0104
			0.0004		0.0009	0.0009	0.0011			0.0005	0.0006
O1	2/3	1/3	1.2378	1	0.027	0.027	0.000	0	0	0.014	0.018
			0.0012		0.003	0.003	0.003			0.001	0.002
O2	0.1777	0.1019	0.9436	1	0.009	0.032	0.009	0.004	0.005	0.003	0.0198
	0.0006	0.0006	0.0006		0.002	0.002	0.002	0.001	0.002	0.002	0.0010
O3	0.4852	0.2546	0.9532	1	0.018	0.038	0.009	–0.009	–0.006	0.014	0.0218
	0.0008	0.0007	0.0006		0.002	0.003	0.002	0.002	0.001	0.002	0.0010
O4	0	0	1.2382	1	0.031	0.031	0.000	0	0	0.015	0.021
			0.0012		0.003	0.003	0.003			0.002	0.002
O5	0.1741	0.0746	0.5526	1	0.010	0.028	0.013	0.002	–0.003	0.005	0.0190
	0.0007	0.0006	0.0006		0.002	0.002	0.002	0.002	0.001	0.002	0.0009
O6	0.4893	0.2318	0.5436	1	0.023	0.024	0.020	0.001	0.006	0.009	0.0235
	0.0008	0.0006	0.0007		0.003	0.002	0.002	0.002	0.002	0.002	0.0011
O7	0.3328	0.3796	0.7136	1	0.023	0.021	0.018	0.004	0.000	0.014	0.0192
	0.0006	0.0005	0.0007		0.002	0.002	0.002	0.002	0.002	0.002	0.0009
O8	0.3321	0.9514	0.7812	1	0.028	0.024	0.025	–0.004	0.000	0.010	0.027
	0.0007	0.0006	0.0008		0.002	0.002	0.003	0.002	0.002	0.002	0.001
OW9	0.3320	0.3998	0.3088	1	0.046	0.032	0.030	0.017	0.004	0.020	0.036
	0.0007	0.0006	0.0008		0.003	0.002	0.002	0.002	0.002	0.002	0.001
OW10	0.0748	0.4065	0.1923	1	0.070	0.052	0.023	0.001	0.004	0.036	0.046
	0.0007	0.0007	0.0008		0.004	0.004	0.002	0.002	0.002	0.003	0.002

equatorial Nb–O distances of 1.97–1.99 Å, a short apical Nb–O distance of 1.77 Å, and a long apical Nb–H_2O distance of 2.36 Å (Sokolova & Hawthorne 2004). The short *Nb*–O bonds, which correspond to displacement of *Nb* from the equatorial plane, likely represent double (π) bonds whereas the more typical *Nb*–O distances represent single (σ) bonds. The displacement of highly charged cations like Nb^{5+} from the equatorial plane has been discussed by Megaw (1968a, b) and Piilonen *et al.* (2006). In short, small cations of high charge in octahe-

TABLE 5. INTERATOMIC DISTANCES (Å) IN LAURENTIANITE

Na$O_6(H_2O)_2$ Polyhedron			*Nb*(1)$O_5(H_2O)$ Octahedron		
Na	–OW9	2.377(7)	*Nb*1	–O8	1.780(6)
	–OW10	2.409(8)		–O5	1.949(5)
	–O3	2.430(8)		–O2	1.974(5)
	–O2	2.478(8)		–O6	1.983(6)
	–O6	2.514(9)		–O3	2.005(6)
	–O5	2.555(8)		–O7	2.498(6)
	–O4	2.844(5)	<*Nb*1	–O>	2.032
	–O1	2.894(5)			
<*Na*	–O>	2.563			
Nb(2)$O_5(H_2O)$ Octahedron			*Si*(1)O_4 Tetrahedron		
*Nb*2	–O7	1.776(5)	*Si*1	–O1	1.555(9)
	–O5	1.944(6)		O3x3	1.627(6)
	–O2	1.968(5)	<*Si*1	–O>	1.609
	–O6	1.982(6)			
	–O3	2.010(6)	*Si*(2)O_4 Tetrahedron		
	–O8	2.502(6)			
<*Nb*2	–O>	2.030	*Si*2	O6x3	1.598(7)
				–O1	1.685(9)
			<*Si*2	–O>	1.620
Si(3)O_4 Tetrahedron			*Si*(4)O_4 Tetrahedron		
	–O4	1.556(9)	*Si*4	O5x3	1.591(6)
*Si*3					
	O2x3	1.616(4)		–O4	1.680(9)
<*Si*3	–O>	1.601	<*Si*4	–O>	1.613

Inferred H-bonding relationships

	O_D...O_A (Å)	O_D–O_A–O_A (°)
O7–O8	2.869(9)	118.3(2)
	2.969(9)	118.8(2)
O7–OW9	2.842(5)	97.1(2)
O8–OW10	2.891(6)	102.6(2)
OW9–OW10	2.716(10)	115.0(2)
	2.757(9)	115.7(3)

TABLE 6A. BOND-VALENCE* TABLE (*v.u.*) FOR LAURENTIANITE: ASSUMING *Nb*1 = □, *Nb*2 =, Nb^{5+}, *O*7 = O^{2-} and *O*8 = H_2O

	Na	*Nb*1	*Nb*2	*Si*1	*Si*2	*Si*3	*Si*4	SUM	*H*1	*H*2	*H*3	*H*4	*H*5	*H*6	*H*7	*H*8	SUM
O1	0.05			1.20	0.85			2.10									2.10
O2	0.15		0.86			$1.02^{x3\downarrow}$		2.03									2.03
O3	0.16		0.77	$0.99^{x3\downarrow}$				1.92									1.92
O4	0.05					1.20	0.86	2.11									2.11
O5	0.12		0.92				$1.09^{x3\downarrow}$	2.13									2.13
O6	0.13		0.82		$1.07^{x3\downarrow}$			2.02									2.02
O7			1.44					1.44			0.20	0.20	0.20				2.04
O8			0.20					0.20			0.80	0.80			0.20		2.00
OW9	0.19							0.19					0.80	0.80		0.20	1.99
OW10	0.17							0.17						0.20	0.80	0.80	1.97
SUM	1.02		5.01	4.17	4.06	4.26	4.13				1.00	1.00	1.00	1.00	1.00	1.00	

*Calculated using parameters from Brese & O'Keeffe (1991)

TABLE 6B. BOND-VALENCE TABLE (*v.u.*) FOR LAURENTIANITE: ASSUMING *Nb*1 = Nb^{5+}, *Nb*2 = □, *O*7 = H_2O and *O*8 = O^{2-}

	Na	*Nb*1	*Nb*2	*Si*1	*Si*2	*Si*3	*Si*4	SUM	*H*1	*H*2	*H*3	*H*4	*H*5	*H*6	*H*7	*H*8	SUM
O1	0.05			1.20	0.85			2.10									2.10
O2	0.15	0.84				1.02$^{x3\downarrow}$		2.01									2.01
O3	0.16	0.78		0.99$^{x3\downarrow}$				1.93									1.93
O4	0.05					1.20	0.86	2.11									2.11
O5	0.12	0.90					1.09$^{x3\downarrow}$	2.11									2.11
O6	0.13	0.82			1.07$^{x3\downarrow}$			2.03									2.03
O7		0.20						0.20	0.80	0.80			0.20				2.00
O8		1.42						1.42	0.20	0.20					0.20		2.02
OW9	0.19							0.19					0.80	0.80		0.20	1.99
OW10	0.17							0.17						0.20	0.80	0.80	1.97
SUM	1.02	4.96		4.08	4.09	4.26	4.19		1.00	1.00			1.00	1.00	1.00	1.00	

*Calculated using parameters from Brese & O'Keeffe (1991).

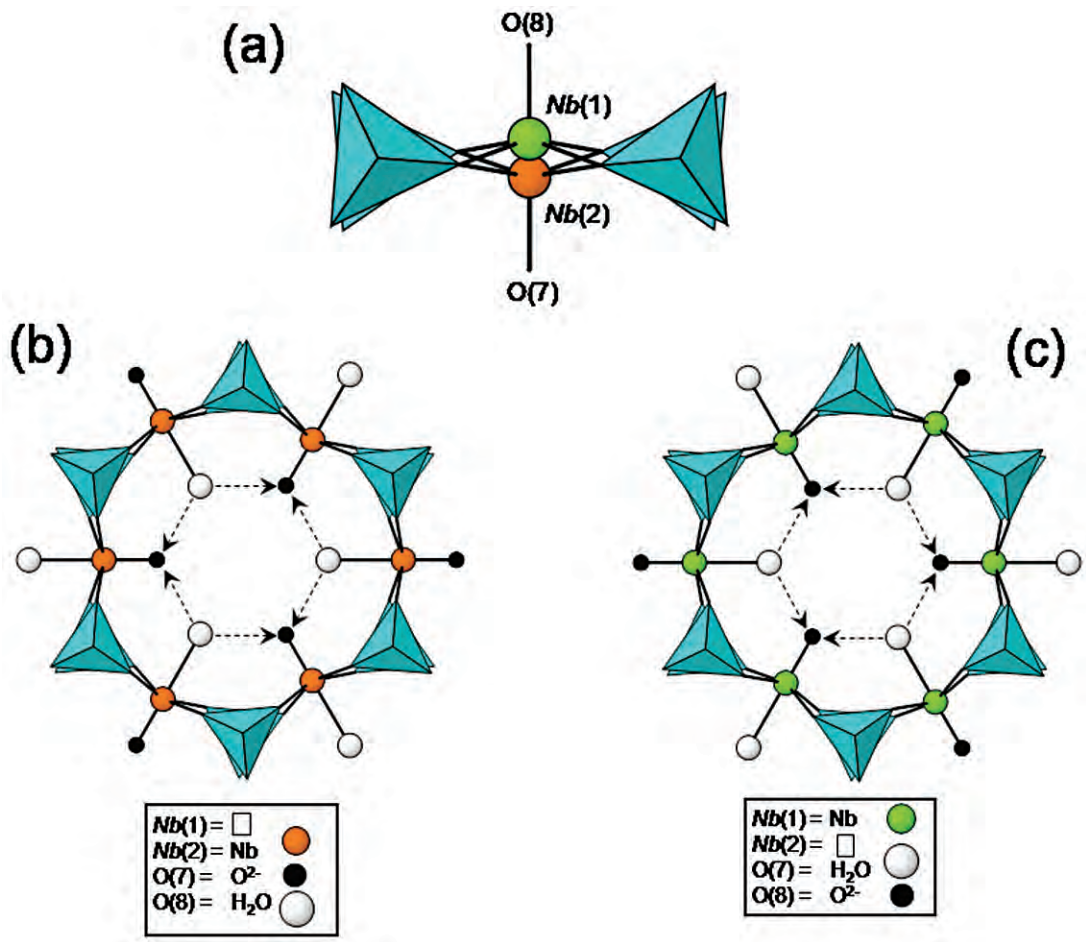

FIG. 3. The local configuration around Nb at ~z = ¾: (a) viewed perpendicular to [001]; (b) viewed parallel to [001] showing one scenario with *Nb*1 vacant and *Nb*2 occupied; (c) the second scenario, with *Nb*1 occupied and *Nb*2 vacant. Weak H-bonds from H_2O groups are shown in dashed lines. The SiO_4 tetrahedra are shown in light blue and the apical oxygens of the $NbO_5(H_2O)$ octahedron, O7 and O8, are indicated.

dral coordination may undergo off-center displacements if their effective radius is such that the unstressed *M*–O bond length is less than $1/\sqrt{2}$ times the diameter of the anion. This leads to significant O–O repulsion that in turn strains the O–*M*–O bond. Reduction of such strain can be achieved by movement of the cation from the equatorial plane (*i.e.*, off-center displacement) that in turn leads to a relaxation of the O–O edges.

While the equatorial Nb–O bonds in the $NbO_5(H_2O)$ octahedron are typical, the apical bonds with O7 and O8 are highly unusual in that their asymmetry gives rise to a rather unique cation-anion configuration. Examination of the local environment around the *Nb* sites reveals that the identity of the anion at the O7 and O8 sites (*i.e.*, O^{2-} or H_2O) is dependent on the occupancy of the *Nb* sites (*i.e.*, *Nb*1 or *Nb*2). When *Nb*1 is occupied, the bond to O7 is ~2.50 Å, and the associated bond valence is only ~0.2 *v.u.*; thus O7 will be occupied by an H_2O group. Simultaneously, the *Nb*1 bond to O8 is exceedingly short ~1.78 Å, and the associated bond valence is ~1.4 *v.u.*; thus O8 is occupied by O^{2-}. Both *Nb*1 and *Nb*2 cannot be occupied simultaneously, so when *Nb*2 is occupied on the other side of the equatorial plane, the situation is reversed, and O7 = O^{2-} and O8 = H_2O. As the *Nb*1 and *Nb*2 sites are approximately equally populated by Nb^{5+} this leads to both *O*7 and *O*8 having, on average, identical, mixed compositions of $O^{2-}{}_{0.5}(H_2O)_{0.5}$. Locally, the Nb^{5+} atom will always be octahedrally coordinated by $O_5(H_2O)$. It is possible that local Nb–(O^{2-}/H_2O) ordering may be responsible for the apparent supercell observed along *c* (*i.e.*, ~6*c*); however, we were unable to satisfactorily refine such an arrangement. As a test of the overall significance of the supercell reflections, the 3-dimensional single crystal X-ray intensities (indexed on the 10 × 10 × 42 Å cell) were collapsed onto a 2-dimensional representative powder trace. From this, only four superlattice peaks could be identified, all with relative intensities of ~1 %, none of which could be identified on our experimental powder pattern.

There is one *Na* site in eight-fold coordination in the form of a $NaO_6(H_2O)_2$ polyhedron with distances ranging from 2.377 to 2.894 Å (shorter distances corresponding to Na–H_2O bonds) and an average <Na–(O, H_2O)> bond distance of 2.563 Å (Table 5).

Nb ordering and associated hydrogen bonding

The *Nb*1 and *Nb*2 positions, relative to the equatorial shared anions of the flanking SiO_4 groups and apical O7 and O8 anions, are shown in Figure 3a. Bearing in mind that both *Nb* sites cannot be occupied simultaneously, if one considers only the *Nb*2 site within a Nb–Si ring to be occupied, then the nearest O7 site (Nb2–O7 = ~1.78 A or ~1.4 *v.u.*) must be occupied by O^{2-} and the nearest O8 position (*Nb*2–O8 = ~2.50 A or ~0.2 *v.u.*) must be occupied by an H_2O group (Figure 3b). Moving around the ring, it becomes apparent that if all the Nb atoms within a single ring occupy the *Nb*2 sites, then all O7 sites will be occupied by O^{2-} and all the O8 sites by H_2O groups, in order to preserve a balanced donor-acceptor relation between neighboring O7/O8 anions. This local ring configuration results in each O^{2-} at O7 receiving two neighboring H-bonds from two adjacent H_2O groups at O8. If instead the *Nb*1 site is occupied, the opposite configuration will exist, *i.e.*, all O7 sites will be occupied by H_2O groups and all O8 sites by O^{2-} (Fig. 3c). These two opposing configurations (Figs. 3b, c) occur with near equal frequencies in laurentianite, such that each O7 and O8 site may be considered as having a composition of, on average, $O^{2-}{}_{1/2}/H_2O_{1/2}$. It must be remembered that when a single *Nb* site is occupied (*i.e.*, either *Nb*1 or *Nb*2), all the same *Nb* sites in adjacent Nb–Si rings at the same height along [001] are similarly occupied, giving rise to a Nb-ordering pattern that propagates outward within a given (001) plane. In other words, within a select (001) Nb-slab within laurentianite, each Nb atom has a fixed O^{2-} atom and H_2O molecule associated with it and it is only when moving further along [001] that an apparent blending (disordering) of O^{2-} and H_2O anions occurs. Whether a particular O7/O8 anion operates as an H-bond donor or acceptor depends on the relative positioning of an Nb atom: if *Nb*2 is occupied, then the O7 site is occupied by O^{2-}, receiving ~1.4 *v.u.* from *Nb*2 and ~0.2 *v.u.* (×2) from the two H-bonds of the two adjacent H_2O groups at O8 (Fig. 3b, Table 6a), for a bond valence sum of 1.8 *v.u.* At the same time, the adjacent H_2O groups at O8 receive ~0.2 *v.u.* from *Nb*2 and ~0.8 *v.u.* (×2) from the two H atoms (Fig. 3b, Table 6a), giving a bond valence sum also of 1.8 *v.u.* A similar, but opposite, situation will exist when the *Nb*1 site is occupied (Fig. 3c, Table 6b). Both arrangements necessarily lead to the O7 and O8 anions being slightly under-bonded (~ Σ1.8 *v.u.*), but this is remedied by the additional receivership of a single H-bond from the H_2O group at OW9 or OW10, respectively (Tables 6a, 6b). Thus, a satisfactory bond valence sum at the apical O^{2-} anions (O7 or O8) is achieved by a combination of the short Nb–O bond contribution and receivership of a total of three H-bonds and a similar bond valence sum for the apical H_2O groups (O8 or O7) via a long Nb–O bond contribution, in combination with two attached H atoms, and receivership of a single H-bond.

The Nb atoms are centered at ~z = ¾ and moving down the channel to a height of ~z = ¼, [where the Na atoms are in the (001) plane], it can be seen that these are both flanked by neighboring Si_2O_7 groups and bonded to the OW9 and OW10 H_2O groups (Fig. 4). Note that the O7 and O8 anions (not shown in Fig. 4) lie immediately above and below the OW9 and OW10 positions, respectively (this can be seen in Fig. 5 in a cut-away view along the channel wall). Note that in Figure 5, a given O7 site is closer to an OW9 site situ-

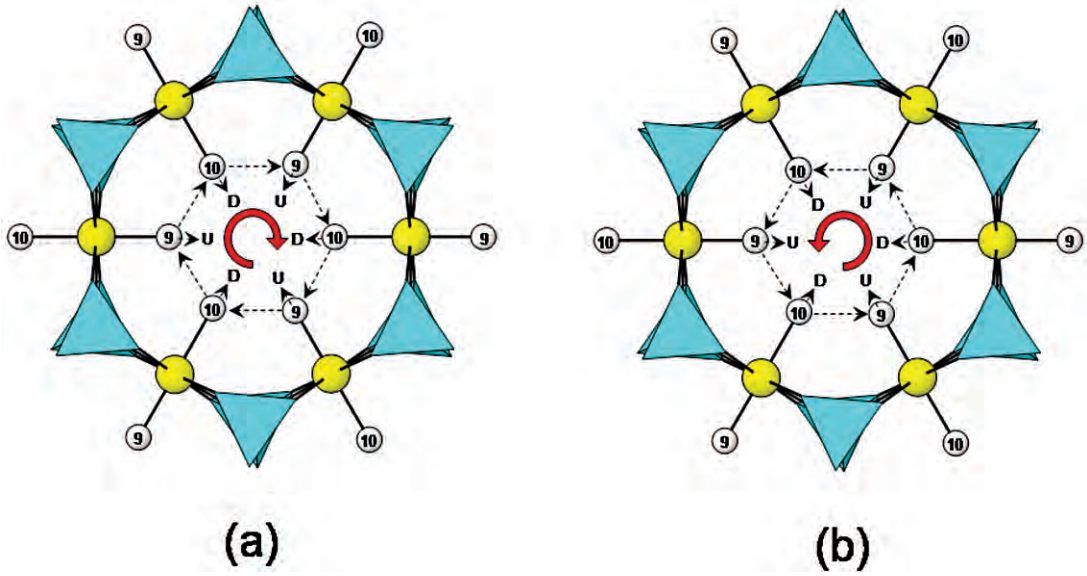

FIG. 4. The local environment around Na at ~z = ¼ viewed parallel to [001] showing the H_2O groups OW9 and OW10. Potential H-bonding schemes are shown in: (a) (clockwise) and (b) (counter clockwise).

ated below (~2.8 Å separation) and more distant from the OW9 site lying above (~4.1 Å separation), with the opposite situation existing between O8 and OW10. The shorter OW9…O7 and OW10…O8 approaches of ~2.8 Å are reasonable O_D–O_A distances and we have assigned H-bonds from OW9 and OW10 to O7 and O8, respectively (Tables 6a, b). Note that the O7 and O8 receivership of these H-bonds occurs regardless of the specific anion identity at O7 or O8. The relative direction of the H-bond from OW9 and OW10 along [001] (*i.e.*, up or down) is shown in Figures 4a and b with the corresponding letters *U* and *D*. The other H-bond originating from the H_2O group at OW9 and OW10 is directed at one of the two neighboring H_2O groups (OW10 or OW9) inside the ring. When comparing Figures 4a and b, a circular propagation of H-bonds around the ring in either a clockwise or counter clockwise direction results. This is also shown on Figure 5 by varying the direction of H-bonds away from the various OW9 positions along [001]. There are no restrictions imposed by the structure in terms of the relative rotation of H-bonds (*i.e.*, clockwise *versus* counter clockwise) within a ring or between rings. The H_2O groups at OW9 and OW10 then each receive a single H-bond (~0.2 *v.u.*) from either an OW10 or OW9 H_2O group (respectively), in addition to the bond valence contributions from the Na (~0.2 *v.u.*) and two H atoms (~0.8 *v.u.* ×2), thus giving acceptable bond valence sums of 2 *v.u* (Tables 6a, b). Importantly, the *Nb*1/*Nb*2–O7/O8 (O^{2-}/H_2O) local ordering does not couple to the local H-bonding above and below (*i.e.*, from OW9 and OW10), and ordering in the two regions of the structure can operate independently. Considering that both ordering mechanisms are in operation and given the influence each would have on resulting X-ray diffraction intensities, it is more likely that the former (*i.e.*, *Nb*1/*Nb*2–O7/O8) could be responsible for the larger cell (*i.e.*, 6*c*) that was alluded to earlier.

Structure Topology

The basic motif present in the crystal structure of laurentianite is a five-membered pinwheel of composition $[Nb_3Si_2O_{17}(H_2O)_3]^{-11}$ consisting of three $NbO_5(H_2O)$ octahedra linked to two SiO_4 tetrahedra (Fig. 6a, b). Individual Nb–Si pinwheels are linked into more complex, 18-membered hexagonal rings of composition $[Nb_6Si_{12}O_{54}(H_2O)_6]^{30-}$, which in turn are linked to form a Nb–Si layer in the [001] plane (Fig. 7). The Nb–Si layers are then joined along [001] through shared SiO_4 tetrahedra to produce a three-dimensional structure. Alternatively, the crystal structure can also be considered as being layered along [001], with a silicate layer of (Si_2O_7) dimers and a layer of isolated $NbO_5(H_2O)$ octahedra, the two layers alternating along [001] (Fig. 8). Laurentianite lacks any discernible cleavage, implying that bonding involving the (Si_2O_7) dimers and $NbO_5(H_2O)$ octahedra must be both strong and reasonably equivalent in directions both parallel and perpendicular to [001]. Sodium atoms are restricted to

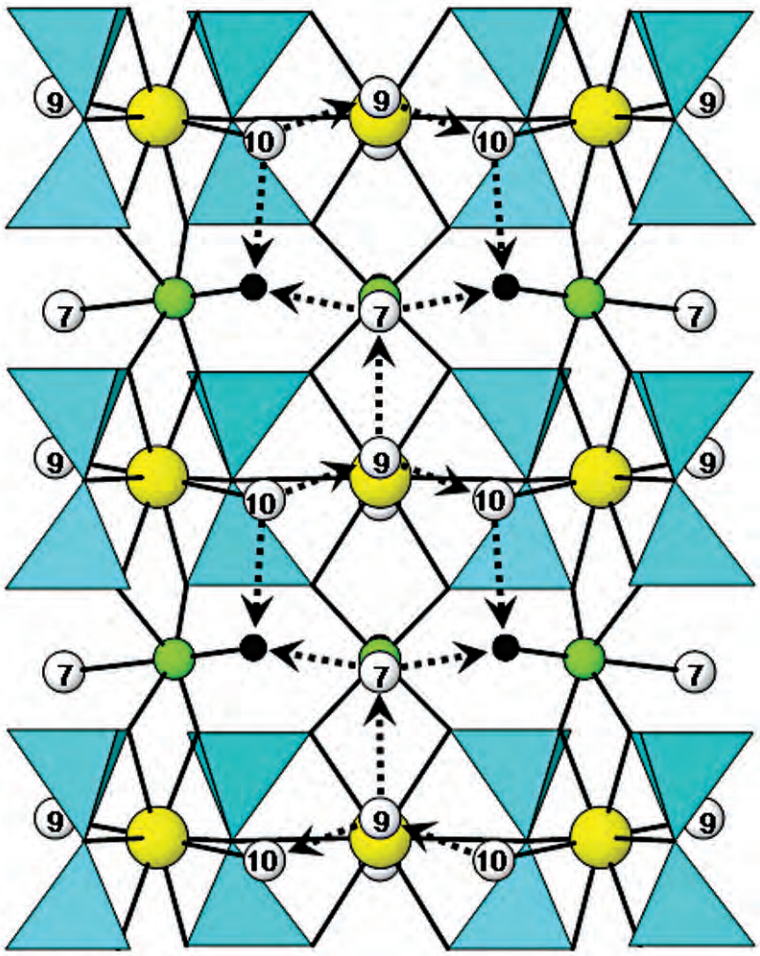

FIG. 5. H-bonding scenarios in laurentianite, viewed perpendicular to [001], showing weak contributions of H_2O groups OW9 and OW10 to O7 (H_2O; labeled) and O8 (O^{2-}; black sphere, not labeled).

the silicate layer, occupying sites that almost directly overlie those of Nb, but are displaced by ~½ + *z* (Fig. 9).

Related Structures

Neither the observed X-ray powder diffraction pattern nor the crystal structure of laurentianite match those of any known mineral or synthetic phase. When the major structural features of laurentianite are considered, there are some distant similarities between these and those observed in both traskite [$(Ba,Ca)_9(Fe^{2+},Mn)_2Ti_2(SiO_3)_{12}(OH,Cl,F)_6{\cdot}6H_2O$; Malinovskii *et al.* 1976] and asbecasite ($Ca_3TiAs_6Be_2Si_2O_{20}$; Sacerdoti *et al.* 1993). The crystal structure of traskite may be considered as being based on twelve-membered rings as in laurentianite, but in traskite, these are true silicate rings, whereas in laurentianite, they are heteropolyhedral, being composed of both SiO_4 tetrahedra and $NbO_5(H_2O)$ octahedra. While the twelve-membered rings clearly influence the symmetry in both minerals, there is no strict correspondence in the unit-cell parameters between the two, so the similarities between them are necessarily distant. In the crystal structure of asbecasite, layers of $SiBeO_7$ dimers alternate with mixed layers of TiO_6 octahedra and CaO_8 polyhedra along [001]. If one considers the crystal structure of laurentianite in terms of a silicate layer (*i.e.*, the Si_2O_7 dimers) alternating with a layer of $NbO_5(H_2O)$ octahedra, there is a distant relationship between the two.

Origin and Paragenesis

The specific geological environment in which laurentianite developed at Mont Saint-Hilaire is unclear, as the observed mineral assemblage has not, hitherto, been reported at the locality and because samples containing the mineral were not found *in situ*. The dominant mineral on these samples is siderite and as this occurs in high concentrations in vugs within sodalite syenite and in late-stage pegmatites, both are strong candidates as the primary source of this material. The presence of franconite is also relevant; while it may be found in a number of microenvironments (hornfels, nepheline syenite, *etc.*), it is particularly common in sodalite syenite. Thus, the combination of abundant siderite and franconite suggests that the laurentianite-bearing samples likely originated within late-stage vugs in sodalite syenite. However, the presence of abundant, euhedral quartz crystals is inconsistent with the low SiO_2 content of a syenite, thus implying that contamination with more siliceous material must have occurred. It is possible that the interaction of syenite 'melts' with

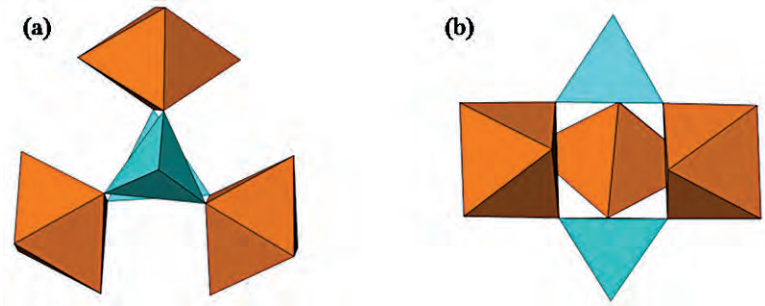

FIG. 6. The five-membered pinwheels of composition $[Nb_3Si_2O_{17}(H_2O)_3]^{-11}$ in laurentianite (a) along [001] and (b) perperdicular to [001]. The $NbO_5(H_2O)$ octahedra are given in orange, the SiO_4 tetrahedra in light blue.

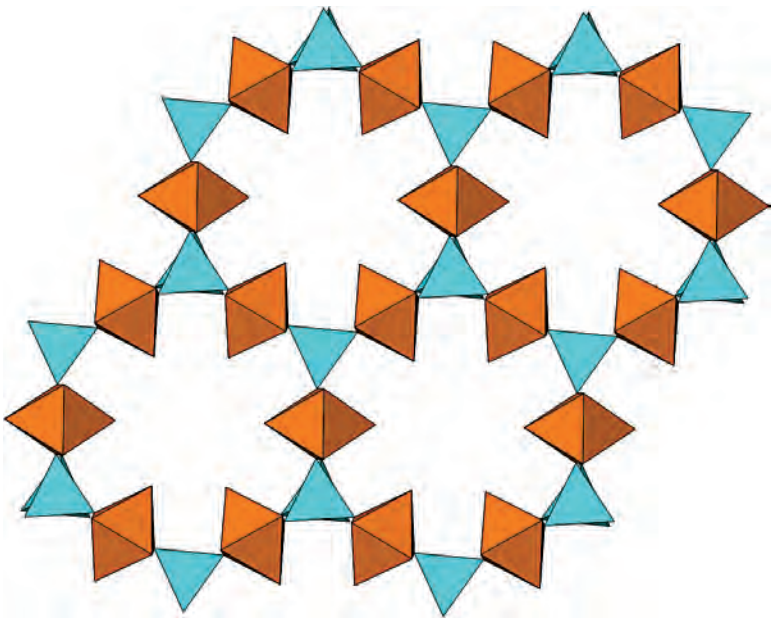

FIG. 7. The 18-membered rings of composition $[Nb_6Si_{12}O_{54}(H_2O)_6]^{30-}$ in laurentianite viewed along [001]. Shading of polyhedra as in Figure 6.

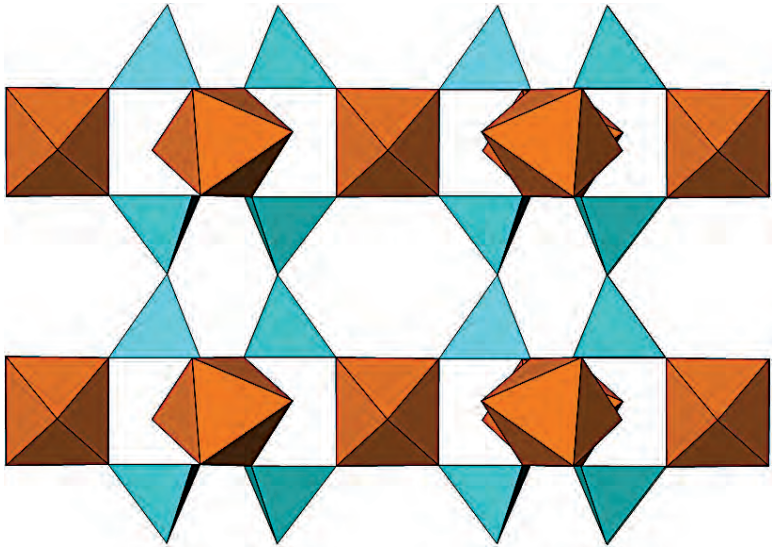

FIG. 8. The crystal structure of laurentianite viewed perpendicular to [001] showing the layers composed of (Si_2O_7) dimers and isolated $NbO_5(H_2O)$octahedra. Shading of polyhedra as in Figure 6.

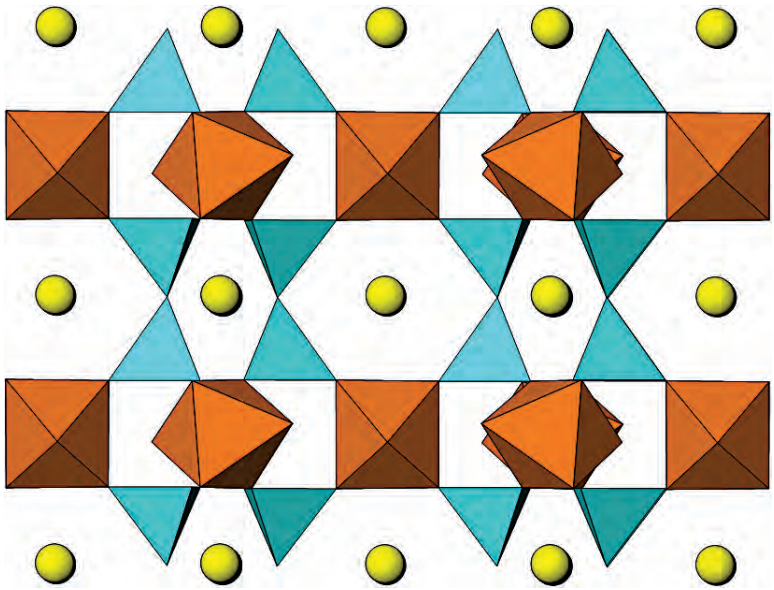

FIG. 9. The crystal structure of laurentianite viewed parallel to [001] showing the positions of Na atoms (yellow spheres).

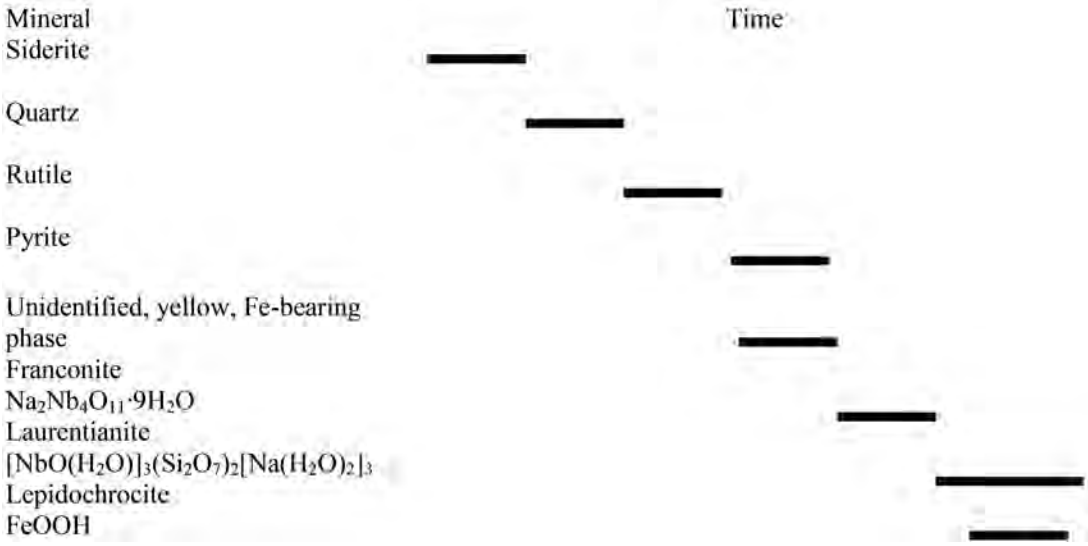

FIG. 10. Mineral paragenesis.

surrounding country rock (which includes siliceous siltstones and shales of the Ordovician Richmond and Lorraine Groups; Currie *et al*. 1986) could have facilitated the release of large amounts of SiO_2 which in turn could explain the abundant quartz that is observed.

Based on examination of the laurentianite-bearing samples, the paragenetic sequence is: siderite → quartz → rutile → pyrite → unidentified, yellow, Fe-bearing phase → franconite → lepidochrocite → laurentianite (Fig. 10). Observations suggest that pyrite and the unidentified yellow Fe-bearing phase likely developed contemporaneously, as did laurentianite and lepidochrocite. In the latter case, laurentianite is typically coated by, and intergrown with, lepidochrocite, developing a reddish coloration as a result (Fig. 1). However, on rare occasions, laurentianite grains are also found that are white to colorless, *i.e.*, are not grown with lepidochrocite, suggesting they may have crystallized just prior to lepidochrocite, albeit close in time.

The presence of lepidochrocite in laurentianite-bearing samples is important as it indicates late-stage alteration, likely resulting from oxidizing, low-to-moderate pH fluids. Lepidocrocite is stable under oxidizing conditions (Eh = 0 to 1.0 V) over a pH range between 4 and 7 (Langmuir & Whittemore 1971). The presence of altered pyrite (likely precursor to lepidochrocite) suggests that the fluids were oxidizing and as this can lead to production of H_2SO_4, a further reduction in the pH of the late-stage fluids would be expected. The fluids are also considered to have been enriched in HF based on the presence of quartz with partially etched crystal faces (Nielsen & Foster 1960; Subramanian 1975).

Finally, the chemistry of secondary hydrous phases such as laurentianite and lepidocrocite indicate that the late-stage fluid was both aqueous in nature and enriched in Na, Fe, and high-field strength elements (HFSE), principally Nb. Although HFSE are usually considered to be immobile, experimental and empirical evidence suggests they may be mobilized under agpaitic conditions such as those found at Mont Saint-Hilaire (Rubin *et al*. 1993, Olivo & Williams-Jones 1999, Salvi *et al*. 2000). Since laurentianite is closely associated with franconite, which contains >75 wt.% Nb_2O_5, the requisite Nb in laurentianite was likely derived *via* the breakdown of franconite, the Si from the dissolution of quartz, and the Na from the breakdown of sodalite, with the addition of H_2O from the fluid which transported these species.

ACKNOWLEDGEMENTS

Our thanks to F.C. Hawthorne (Dept. of Geological Sciences, University of Manitoba) for providing access to the three-circle diffractometer. We also acknowledge the comments made by the Co-Editor, Prof. L.A. Groat, and additionally thank Dr. Groat, Dr. R.C. Peterson, and Ms. M. Parker for their editorial assistance. Financial support for this research was provided through a grant to AMM from the Natural Sciences and Engineering Research Council.

References

Babechuk, M.G. & Kamber, B.S. (2011) An estimate of 1.9 Ga mantle depletion using the high-field-strength elements and Nd–Pb isotopes of ocean floor basalts, Flin Flon Belt, Canada. *Precambrian Research* **189**, 114-139.

Barth, M.G., Mcdonough, W.F., & Rudnick, R.L. (2000) Tracing the budget of Nb and Ta in the continental crust. *Chemical Geology* **165**, 197-213.

Brese, N.E. & O'keeffe, M. (1991) Bond-valence parameters for solids. *Acta Crystallographica* **B47**, 192-197.

Cromer, D.T. & Liberman, D. (1970) Relativistic calculation of anomalous scattering factors for X rays. *The Journal of Physical Chemistry* **53**, 1891-1898.

Cromer, D.T & Mann, J.B. (1968) X-ray scattering factors computed from numerical hartree-fock wave functions. *Acta Crystallographica* **A24**, 321-324.

Currie, K.L., Eby, G.N., & Gittins, J. (1986) The petrology of the Mont Saint-Hilaire compex, southern Quebec: An alkaline gabbro-pyroxenite syenite association. *Lithos* **19**, 65-81.

Dowty, E. (2002) *CRYSCON for Windows and Macintosh Version 1.1*. Shape Software Kingsport, Tennessee, USA.

Jochum, J.P., Stolz, A.J., & Mcorist, G. (2000) Niobium and tantalum in carbonaceous chondrites: Constraints on the solar system and primitive mantle niobium/tantalum, zirconium/niobium and niobium/uranium ratios. *Meteoritics and Planetary Science* **35**, 229-235.

Langmuir, D. & Whittemore, D.O. (1971) Variations in the stability of precipitated ferric oxyhydroxides. *In* Nonequilibrium Systems in Natural Waters (J.D. Hem, ed.). American Chemical Society, (209-233).

Malinovskii, Yu.A., Pobedimskaya, E.A., & Belov, N.V. (1976) Crystal structure of traskite. *Doklady Akademii Nauk SSSR* **21**, 426.

Mandarino, J.A. (1981) The Gladstone–Dale relationship. IV. The compatibility concept and its application. *Canadian Mineralogist* **19**, 441-450.

Megaw, H.D. (1968a) A simple theory of the off center displacement of cation in octahedral environment. *Acta Crystallographica* **B24**, 149-153.

Megaw, H.D. (1968b) The thermal expansion of interatomic bonds, illustrated by experimental evidence from niobates. *Acta Crystallographica* **A24**, 589-604

Nielsen, J.W. & Foster, F.G. (1960) Unusual etch pits in quartz. *American Mineralogist* **45**, 299-310.

Olivo, G.R. & Williams-Jones, A.E. (1999) Hydrothermal REE-rich eudialyte from the Pilanesberg Complex, South Africa. *Canadian Mineralogist* **37**, 653-663.

Piilonen, P.C, Farges, F., Linnen, R.L., Brown Jr., G.E., Pawlak, M., & Pratt, A. (2006) Structural environment of Nb^{5+} in dry and fluid-rich (H_2O, F) silicate glasses: a combined XANES and EXAFS study. *Canadian Mineralogist* **44**, 775-794.

Rocha, J., Brandao, P., Lin, Z., Esculas, A.P., Ferreira, A., & Anderson, M.W. (1996) Synthesis and structural studies of microporous titanium-niobium-silicates with the structure of nenadkevichite. *The Journal of Physical Chemistry* **100**, 14978-14983.

Rubin, J.N., Henry, C.D., & Price, J.G. (1993) The mobility of zirconium and other "immobile" elements during hydrothermal alteration. *Chemical Geology* **110**, 29-47.

Sacerdoti, M., Parodi, G.C., Mottana, A., Maras, A., & Della Ventura, G. (1993) Asbecasite: Crystal structure refinement and crystal chemistry. *Mineralogical Magazine* **57**, 315-322.

Salvi, S., Fontan, F., Monchoux, P., Williams-Jones, A.E., & Moine, B. (2000) Hydrothermal mobilization of high field strength elements in alkaline igneous systems: evidence from the Tamazeght Complex (Morocco). *Economic Geology* **95**, 24-31.

Shannon, R.D. (1976) Revised effective ionic radii and systematic studies of interatomic distances in halides and chalcogenides. *Acta Crystallographica* A32, 751-767.

Sheldrick, G.M. (1997) *SHELXL-97: A computer program for the Refinement of Crystal Structures*. University of Göttingen, Göttingen, Germany.

Sokolova, E. & Hawthorne, F.C. (2004) The crystal chemistry of epistolite. *Canadian Mineralogist* 42, 797-806.

Subramanian, V. (1975) Origin of surface pits on quartz as revealed by scanning electron microscopy. *Journal of Sedimentary Petrology* **45**, 530-534.

Submitted June 28, 2012, manuscript accepted October 12, 2012.